

InAs nanowire hot-electron Josephson transistor

Stefano Roddaro,¹ Andrea Pescaglini,¹ Daniele Ercolani,¹ Lucia Sorba,¹ Francesco Giazotto,¹ and Fabio Beltram^{1,2}

¹NEST, Istituto Nanoscienze-CNR and Scuola Normale Superiore, Piazza S. Silvestro 12, I-56127 Pisa, Italy

²IIT@NEST, Center for Nanotechnology Innovation, Piazza S. Silvestro 12, I-56127 Pisa, Italy

(Dated: October 30, 2018)

At a superconductor (S)-normal metal (N) junction pairing correlations can “leak-out” into the N region. This *proximity effect* [1, 2] modifies the system transport properties and can lead to supercurrent flow in SNS junctions [3]. Recent experimental works showed the potential of semiconductor nanowires (NWs) as building blocks for nanometre-scale devices [4–7], also in combination with superconducting elements [8–12]. Here, we demonstrate an InAs NW Josephson transistor where supercurrent is controlled by hot-quasiparticle injection from normal-metal electrodes. Operational principle is based on the modification of NW electron-energy distribution [13–20] that can yield reduced dissipation and high-switching speed. We shall argue that exploitation of this principle with heterostructured semiconductor NWs opens the way to a host of out-of-equilibrium hybrid-nanodevice concepts [7, 21].

One practical implementation of the present InAs-NW hot-electron Josephson transistor concept is shown in Figure 1a. The SNS junction was fabricated by e-beam lithography starting from an n-doped InAs NW (the N region, for further details see Methods) and comprises two Ti/Al superconducting electrodes placed at a distance $L \simeq 60$ nm (S regions). Control electrodes were fabricated by depositing two additional normal-metal Ti/Au leads at the two ends of the NW. As schematically illustrated by the overlay of Fig. 1a, the N leads are used to drive a dissipative current through the NW thereby tuning Josephson coupling in the S-NW-S structure.

Figure 2a shows a set of typical IV characteristics from one of the measured S-NW-S junctions at equilibrium (i.e., $V_{inj} = 0$) and at different bath temperatures T . High critical currents up to $I_c \simeq 350$ nA (corresponding to a supercurrent density ~ 5.5 kA/cm²) are observed and Josephson coupling typically persists up to about 1 K. Furthermore, from the junction differential-resistance spectra (see Supplementary Materials) we infer a superconducting order parameter $\Delta = 120$ μ eV and a junction normal-state resistance $R_N \simeq 210$ Ω . The $I_c R_N$ product attains values as large as $\simeq 75$ μ eV and indicates the overall success of our junction-fabrication procedure [22]. Based on carrier-density and electron-mobility values (see Methods) we estimate a momentum-relaxation length $\ell \simeq 20$ nm and a diffusion coefficient $D = 0.02$ m²/s. Given the junctions geometrical length L we can estimate the Thouless-energy value, i.e., the characteristic energy scale of the N region, $E_{Th} = \hbar D/L^2 \simeq 4$ meV. These values indicate that our devices can be described within the frame of the diffusive short-junction limit ($L > \ell$ and $\Delta \ll E_{Th}$) [22]. Figure 2b shows the evolution of I_c versus T at $V_{inj} = 0$ for two representative devices D1 and D2. For comparison, the theoretical prediction for an ideal short diffusive SNS junction [22, 23] is also plotted assuming for both devices a supercurrent suppression of the order of 45%. Such a suppression can be expected and probably mainly stems from a residual

barrier at the NW-superconductor contact [22, 24, 25].

Figure 3 demonstrates operation of the NW hot-electron Josephson transistor: supercurrent can be fully suppressed by the application of a voltage bias V_{inj} of the order of a few hundred μ V across the N control line. The overall evolution of the IV characteristics of device D2 as a function of V_{inj} at 370 mK is displayed in Fig. 3a. The corresponding monotonic decay and complete suppression of the critical current I_c vs V_{inj} at different bath temperatures is reported in Figs. 3b and 3c for devices D1 and D2, respectively. Our results show that an injection power of barely ~ 100 pW is sufficient to completely quench the supercurrent. We emphasize that the observation and control of such a robust Josephson effect is made possible by the chosen device architecture, which allows us to use *short* SNS junctions while retaining full tunability of the supercurrent flow. In fact there is no fundamental lower limit to L in our scheme, while other approaches such as, for instance, Josephson field effect transistors (JoFETs) [10, 26, 27], require longer junctions to allow electrostatic gating and avoid excessive screening from the electrodes. These requirements lead to larger control voltages, weaker proximity effect and stray capacitance dictated by the integration of strongly-coupled gates on top of short junctions. Clearly the present operational principle is amenable to all-metal implementations. We should like to stress, however, that our NW-based architecture offers a significant beneficial feature, thanks to the resulting higher impedance in the injection line. The latter reduces the required control power by $\sim 2 - 3$ orders of magnitude with respect to what shown so far in comparable metallic systems [14, 16, 28].

Insight into the working principle of this device can be gained by recalling that in diffusive SNS junctions a continuum spectrum of Andreev bound states is responsible for the supercurrent flow across the structure [13, 22]. Occupation of these supercurrent-carrying states is determined by the quasiparticle energy distribution in the N region which can, in turn, be controlled through the

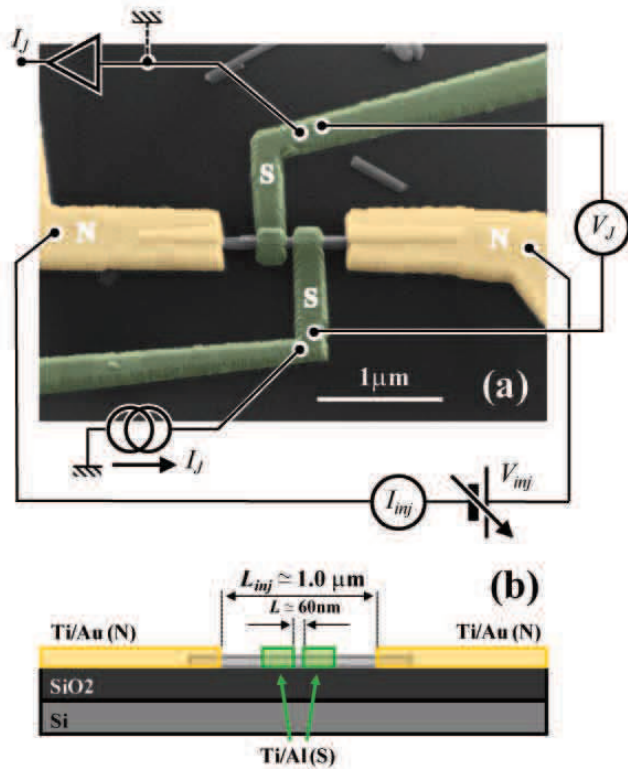


FIG. 1: **InAs NW hot-electron Josephson transistor.** (a) Pseudo-color scanning electron micrograph of one of the measured devices: an InAs NW is coupled to two 250 nm-wide Ti/Al superconducting electrodes (green) to form a ≈ 60 nm-long Josephson junction. The InAs NW is also contacted at its ends to two normal-metal Ti/Au leads (yellow) which are used to control the electron energy distribution in the central region of the junction through quasiparticle injection. As a consequence, the Josephson supercurrent I_J is tuned upon voltage biasing the N control line with V_{inj} . The distance between the two normal-metal electrodes is $L_{inj} \approx 1 \mu\text{m}$. The overlay schematics shows a sketch of the measurement set-up: the supercurrent is detected using a four-wire scheme, while the injection circuit consists of a floating network. (b) Schematic cross-section view of a typical device with some relevant geometrical details. The transistors were fabricated on top of an insulating Si/SiO₂ substrate by electron-beam lithography and metal deposition.

application of a finite bias V_{inj} across the NW [13, 22]. Although a detailed quantitative description of this effect is rather complex, we believe that the dominant physics governing our devices can be captured by considering the experimentally-observed heating of the electron system following current injection. Comparison between Figs. 2a and 3a suggests that upon hot-quasiparticle injection NW electrons can be described by a quasi-equilibrium Fermi-energy distribution characterised by a temperature T_e larger than the bath temperature [21]. Thanks to the experimental data available, we can convert the measured $I_c(V_{inj})$ values into $T_e(V_{inj})$ by using the mea-

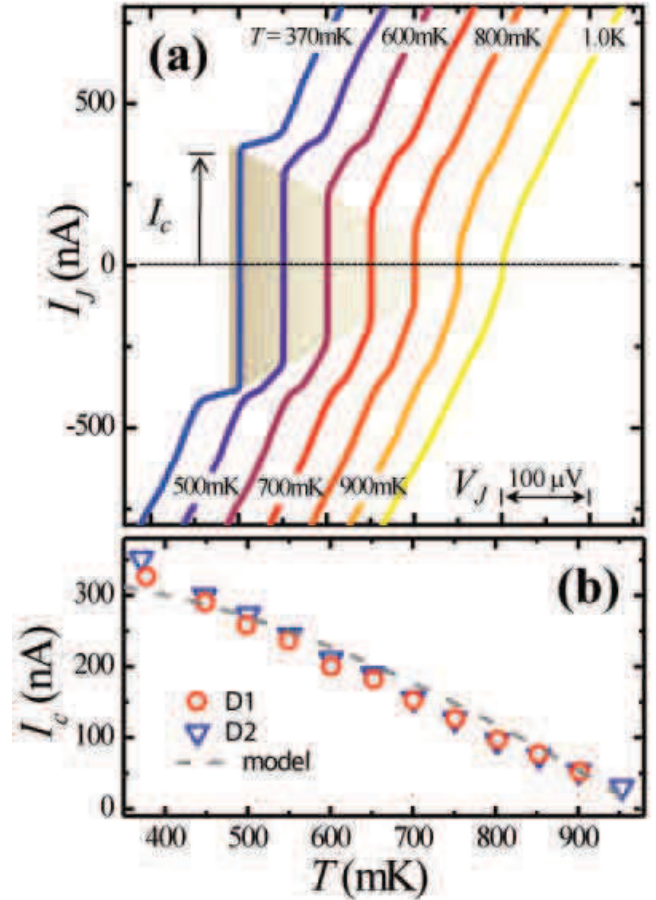


FIG. 2: **Temperature dependence of the Josephson current.** (a) The current-voltage characteristics I_J vs V_J of device D2 demonstrate the presence of dissipationless transport up to a temperature $T \approx 1$ K. I_c is the critical current of the junction, and the hatched area provides a guide to the eye to emphasize the supercurrent suppression as a function of temperature. The curves are horizontally shifted for clarity. (b) Evolution of the measured equilibrium critical current I_c as a function of bath temperature T for two representative devices (D1-red circles, D2-blue triangles). Dashed line is the theoretical prediction for an ideal short diffusive SNS junction. The absence of a clear saturation of $I_c(T)$ suggests that higher critical currents could be observed at lower temperature. The junction normal-state resistance is $R_N \approx 220 \Omega$ and $\approx 210 \Omega$ for device D1 and D2, respectively.

sured temperature-calibration data in Fig. 2b, i.e., by exploiting the equilibrium Josephson junction as an electron thermometer [17, 20, 29].

The resulting evolution of the electron temperature T_e is displayed in Fig. 4b and 4c for devices D1 and D2, respectively. T_e values as a function of V_{inj} and T are determined by the steady-state thermal balance of several in-coming and out-going heat fluxes within the device system, as sketched in Fig. 4a. In particu-

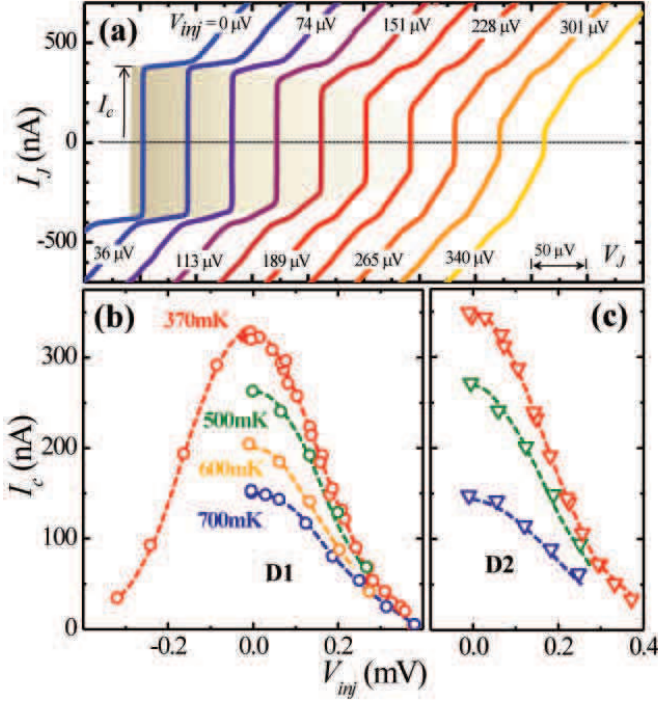


FIG. 3: **Dependence of Josephson current on quasiparticle injection.** (a) Injection of quasiparticles at the Ti/Au electrodes is very effective in tuning the supercurrent flow between the S leads. Few hundred of μV are sufficient to completely quench the Josephson coupling, as it appears in these selected current-voltage characteristics of device D2 measured at $T = 370$ mK. Hatched area provides a guide to the eye which emphasizes the supercurrent suppression as a function of V_{inj} . The curves are horizontally shifted for clarity. (b) and (c) Detailed evolution of the measured critical current I_c as a function of the injection voltage V_{inj} at different bath temperatures T for devices D1 [(b)] and D2 [(c)]. Dashed lines are guides to the eye. Datapoints shown in (b) for negative values of V_{inj} indicate that Josephson current suppression is achieved in a symmetric fashion, regardless the sign of the injection current.

lar, injection of hot carriers and thermal leakage through the lateral N electrodes provide a heat inflow contribution $\dot{Q}_L = \dot{Q}_R = V_{ct}^2/2R_{ct} - L(T_e^2 - T_{ct}^2)/2R_c$, where the parameter L is ideally equal to the Lorentz number $L_0 = 2.44 \times 10^{-8} \text{ W}\Omega/\text{K}^2$ and V_{ct} , T_{ct} and R_{ct} represent the voltage drop, the temperature and the contact resistance, respectively. Although current injection in the control line can in principle lead to a temperature gradient along the NW, we assume the latter to be described as lumped resistor R_w characterized by an average electronic temperature T_e . Furthermore, Joule dissipation within the NW itself is taken into account through the additional term $\dot{Q}_{Joule} = V_w^2/R_w$, where V_w represents the voltage drop across the NW. These contributions can

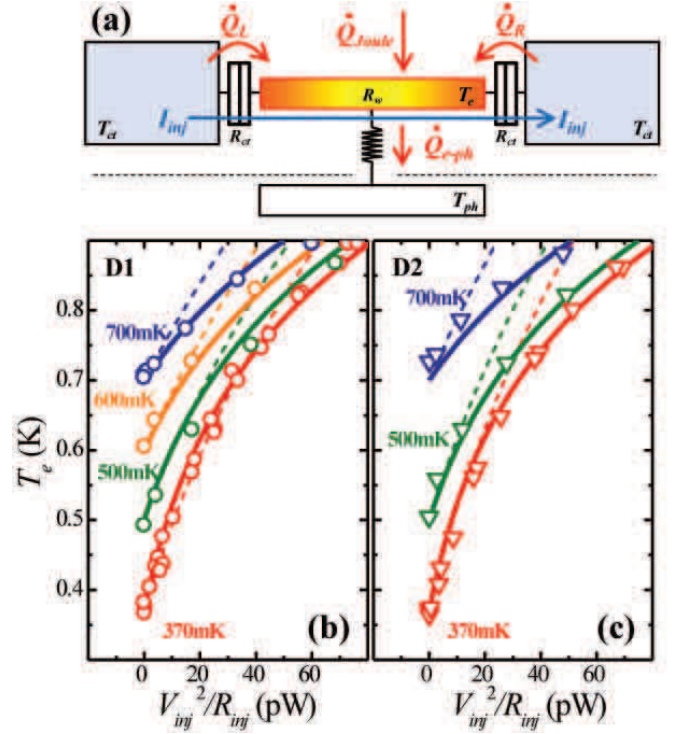


FIG. 4: **Thermal budget analysis of the InAs NW Josephson transistors.** (a) The temperature increase in the electron system of the InAs NW caused by quasiparticle injection is determined by the steady-state balance between in-coming and out-going heat flows in the device. The key ones are: Joule heating (\dot{Q}_{Joule}), heat leakage through the metallic contacts ($\dot{Q}_{L,R}$) and heat exchange between electrons and acoustic phonons (\dot{Q}_{e-ph}). The NW phonon subsystem is assumed to reside at the same temperature as the thermal bath. T_{ph} and T_{ct} represent the phonon and N leads temperatures, respectively, whereas R_w and R_{ct} denote the resistances of the NW and the contacts, respectively. Panels (b) and (c): using the equilibrium I_c vs T characteristics shown in Fig. 2 as a thermometer, we extract the electron temperature T_e as a function of the injection bias V_{inj} at different bath temperatures T for device D1 [(b)] and D2 [(c)]. R_{inj} is the total resistance of the injection line (1.05 k Ω and 1.28 k Ω for device D1 and D2, respectively). Based on statistical data acquired on several junctions of different length we estimated the contact resistance to be $R_{ct} \simeq 100 \Omega$. The experimental behavior is then compared to the phenomenological model sketched in panel (a). The best fit is indicated by the continuous lines whereas the dashed ones correspond to the limit where electron-phonon interaction is neglected.

be recast in terms of the measured injection voltage V_{inj} and total resistance of the injection line R_{inj} by defining the lever arms $V_{ct} = \alpha_{ct}V_{inj}$ and $V_w = \alpha_w V_{inj}$ with the constraint $\alpha_w = 1 - 2\alpha_{ct}$. Similarly, it is possible to define $R_{ct} = \alpha_{ct}R_{inj}$ and $R_w = \alpha_w R_{inj}$. This leads to

$$\dot{Q}_L + \dot{Q}_R + \dot{Q}_{Joule} = \frac{(1 - \alpha_c)V_{inj}^2}{R_{inj}} - \frac{L(T_e^2 - T^2)}{\alpha_c R_{inj}}, \quad (1)$$

where we set $T_{ct} = T$. The other main relaxation mechanism which is expected to play a role in our structures is heat exchange between electrons and acoustic phonons (\dot{Q}_{e-ph}) in the NW. To this end we make the simplifying assumption that $\dot{Q}_{e-ph} = \Sigma V(T_e^5 - T_{ph}^5)$, which holds for bulk metals at low temperatures (i.e., typically below ~ 1 K), where Σ is a material-dependent constant [21], V is the NW volume and T_{ph} is the phonon temperature in the nanostructure. Since 70-80% of the NWs are covered by electrodes (see Fig. 1a), we also assume that $T_{ph} = T$, i.e., NW phonons thermalize at the Si-substrate and N-leads common bath temperature. Based on all this, we use

$$\dot{Q}_L + \dot{Q}_R + \dot{Q}_{Joule} - \dot{Q}_{e-ph} = 0 \quad (2)$$

to fit the data collected on devices D1 and D2.

Equation (2) well describes the observed behaviour, as visible in Fig. 4b and 4c. α_{ct} is estimated $\simeq 0.1$ based on transport data on wires of different lengths; we note that its value rescales the extracted best-fitting parameters L and ΣV , but nevertheless does not modify the best-fit curves. We obtain $L = 5.1 \pm 0.5 \times 10^{-9}$ W Ω /K² and $\Sigma = 4.7 \pm 0.3 \times 10^9$ W/K⁵m³, using the NW volume $V = 1.6 \times 10^{-20}$ m³. We note that our estimate of Σ is comparable to values typical of bulk metallic films [21]. Furthermore, although the T^2 term in Eq. 2 cannot properly account alone for the observed behaviour (see dashed lines in Figs. 4b and 4c), the precise relative contribution of lead and phonon thermal leakage is rather delicate to estimate owing to the correlation between the two fitting parameters.

We should finally like to comment on two important figures of merit of the transistor: its power gain and speed of operation. Even if the former is lacking in the present non-optimized devices, it can be made sizable by tuning the ratio between R_{inj} and R_N [13], i.e. by fabricating sufficiently-long control lines. Concerning speed, switching time τ is determined by how fast an out-of-equilibrium electron energy distribution can be established in the NW [14, 18]; in our case we estimate $\tau = L_{inj}^2/D \approx 50$ ps, which can be decreased by shortening L_{inj} or increasing D .

In light of possible applications, the present InAs NW-based hot-electron Josephson transistor concept offers a number of attracting features: (i) a large, yet tunable, critical supercurrent; (ii) the possibility to achieve large power gains in optimized devices; (iii) a high operating frequency (easily up to ~ 100 GHz); (iv) a reduced dissipation (~ 100 pW or below), ideal for low-temperature applications; (v) the possibility to combine the Josephson effect with custom quantum structures defined during the NW growth. The adoption of self-assembled nanostructures as the core element of this class of devices thus paves the way to rather broad opportunities since it allows the design and growth of epitaxial quantum systems characterized by atomically-defined potential pro-

files [6, 30], a crucial element for several innovative out-of-equilibrium nanodevice schemes [7, 20, 21].

We gratefully acknowledge R. Fazio, H. Linke, J. Matthews, F. Taddei and H. Xu for fruitful discussions. The work for partially supported by the INFN-CNR Seed projects ‘‘Acoustoelectrics on Self-Assembled One-dimensional Semiconductors’’ and ‘‘Quantum-Dot Refrigeration: Accessing the μ K Regime in Solid-State Nanosystems’’, and by the NanoSciERA project ‘‘NanoFridge’’.

METHODS

Fabrication details of InAs NW devices and measurement set-up. Selenium doped NWs were grown by chemical beam epitaxy on a InAs 111B substrate. Gold catalyst particles were formed by thermal dewetting (at 520°C for 20 min) of a 0.5 nm thick Au film under TBA flux. NWs were grown for 2 hours at 420 °C using TBA (2.0 Torr), TMI (0.3 Torr) and DTBSe (0.4 Torr). NWs had typically a diameter $d = 90 \pm 10$ nm and length $\simeq 2.5 \mu\text{m}$. Transport parameters were estimated over an ensemble of nominally identical 1 μm -long NW field effect transistors using a charge control model [30] and a numerical evaluation of the gate capacitance. Carrier density was estimated to be $n = 1.8 \pm 0.8 \times 10^{19}$ cm⁻³ and electron mobility $\mu = 300 \pm 100$ cm²/Vs. Hot-electron Josephson transistors were fabricated using a technique of dry cleavage of the NWs onto Si/SiO₂ substrates (500 nm oxide on intrinsic Si). Contacts were obtained by a two-step aligned process: thermal evaporation of Ti/Au (10/80 nm) was performed first and followed by e-beam deposition of Ti/Al (10/80 nm). In order to obtain transparent metal-NW contacts great care was devoted to the passivation of the semiconductor surface: InAs NWs were treated with a NH₄S_x solution before each evaporation step. The electric characterization was performed by cooling the devices in a filtered ³He refrigerator down to about 370 mK. Current injection at the normal contacts was obtained using a floating biasing source. Currents and voltages were measured using room-temperature preamplifiers.

Theoretical model for a diffusive SNS Josephson junction in the short limit. The measured Josephson critical currents were analyzed by using a model which holds for short diffusive SNS junctions. In this regime the critical supercurrent I_c is expected to scale with the temperature as [22, 23]

$$I_c(T, \phi) = \beta \frac{2\pi \Delta(T) k_B T \cos(\phi/2)}{q R_N} \quad (3)$$

$$\times \sum_n \frac{1}{\Omega_n(T, \phi)} \tan^{-1} \frac{\Delta(T) \sin(\phi/2)}{\Omega_n(T, \phi)}$$

where $\Omega_n(T, \phi) = \sqrt{\Delta^2(T) \cos^2(\phi/2) + \omega_n^2(T)}$, $\omega_n(T) =$

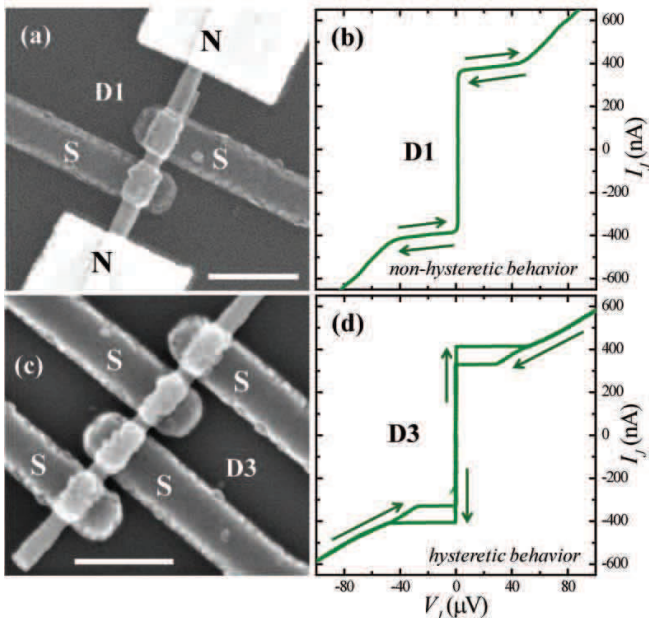


FIG. 5: **Supplementary Fig. S1. Thermal sinks in the Josephson NW transistors.** Non-hysteretic (b) or hysteretic (d) current-voltage characteristics can be obtained depending on the type of contact electrode fabricated on top of the device. The different phenomenology is consequence of the marked difference in terms of thermal sinking of N contacts (a) with respect to S ones (c). The characteristics shown in (b) and (d) were measured at $T = 370$ mK on the device shown in (a) and (c), respectively.

$\pi k_B T(2n + 1)$, and β is a phenomenological suppression coefficient which accounts for the non-ideality of the junction [24, 25]. In the above equation, k_B is the Boltzmann constant, q is the electron charge, R_N is the normal-state resistance of the junction, Δ is the superconducting order parameter, and ϕ is the macroscopic phase difference across the SN boundaries.

SUPPLEMENTARY MATERIALS

Metallic contacts play a crucial role in thermal sinking of the NW device [21]. Figure S1 shows the different behaviour observed on Josephson NW transistors containing either both N and S contacts (Fig. S1 a), or only S ones (Fig. S1 c). In the first case (see Fig. S1 b) we never observed hysteresis in the IV characteristics, while in the second case (see Fig. S1 d) a clear hysteresis developed for devices which exhibit I_c exceeding ~ 100 nA. This different behaviour, which was verified on a number of devices, can be ascribed to the poor thermal conductivity of the superconducting leads in good metallic contact with the NW which act as Andreev *mirrors* for what concerns electronic heat conduction [21]. Hysteresis in

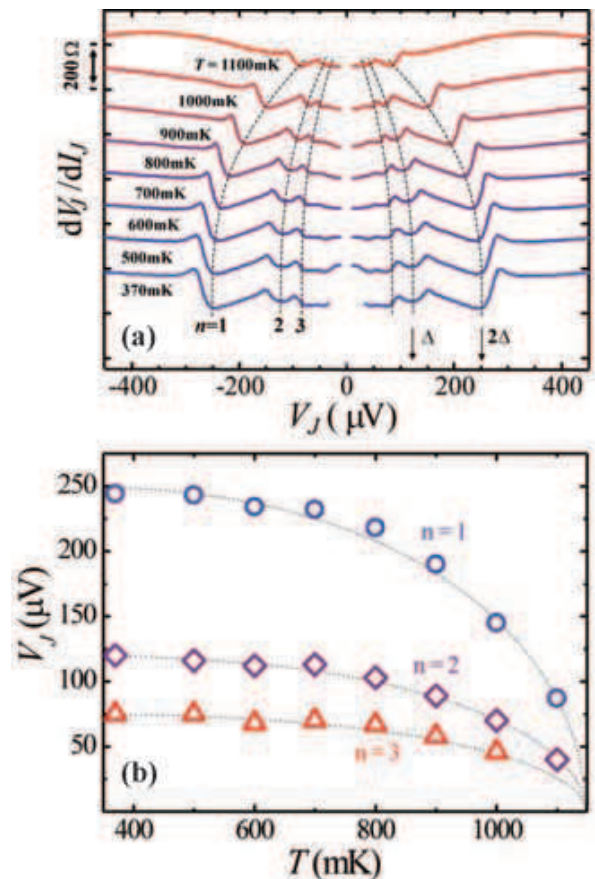


FIG. 6: **Supplementary Fig. S2. Multiple Andreev reflections in the Josephson NW transistor.** (a) Multiple Andreev reflections manifesting in the differential resistance vs voltage characteristics of an InAs S-NW-S junction at selected bath temperatures. Three to four reflection orders are typically visible in the studied devices. The extracted value for the superconducting gap is $\Delta \simeq 120 \mu\text{eV}$. (b) Position of the differential resistance minima for $n = 1, 2$ and 3 as a function of the temperature, and comparison with the Bardeen-Cooper-Schrieffer prediction (dashed lines) for $\Delta(T)$.

mesoscopic SNS junctions is believed to stem from electron heating of the N region once the junction switches to the resistive branch [24]. Our data suggest that the device in Fig. S1c heats up more than that in Fig. S1a when it switches to the dissipative regime.

The differential resistance spectra versus voltage of a typical Josephson NW transistor with all-superconducting leads is visible in Fig. S2a. The plot shows multiple Andreev reflection features [31] occurring at values $V_J = 2e\Delta/n$ with $n = 1, 2$, and 3 for a sequence of different bath temperatures. The extracted value of the gap parameter is $\Delta \simeq 120 \mu\text{eV}$. The V_J position of the minima in dV_J/dI_J as a function of the temperature (see Fig. S2b) closely follows the Bardeen-Cooper-Schrieffer prediction for the superconducting gap [32].

-
- [1] P. G. de Gennes, *Superconductivity of Metals and Alloys* (W. A. Benjamin, 1966).
- [2] A. F. Andreev, Sov. Phys. JETP **19**, 1228 (1964).
- [3] K. K. Likharev, Rev. Mod. Phys. **51**, 101 (1979).
- [4] C. M. Lieber MRS Bulletin 28, 4867491 (2003).
- [5] M. T. Björk, B. J. Ohlsson, T. Sass, A. I. Persson, C. Thelander, M. H. Magnusson, K. Deppert, L. R. Wallenberg, and L. Samuelson, Nano Lett. **2**, 87 (2002).
- [6] S. Roddaro, A. Fuhrer, P. Brusheim, C. Fasth, H. Q. Xu, L. Samuelson, J. Xiang, C. M. Lieber, Phys. Rev. Lett. **101**, 186802 (2008).
- [7] E. A. Hoffmann, H. A. Nilsson, J. E. Matthews, N. Nakpathomkun, A. I. Persson, L. Samuelson, and H. Linke, Nano Lett. **9**, 779 (2009).
- [8] J. Xiang, A. Vidan, M. Tinkham, R. M. Westervelt, C. M. Lieber, Nat. Nanotechnol. **1**, 208 (2006).
- [9] J. van Dam, Y. Nazarov, E. Bakkers, S. De Franceschi, L. Kouwenhoven, Nature **442**, 667 (2006).
- [10] Y.-J. Doh, J. A. van Dam, A. L. Roest, E. P. A. M. Bakkers, L. P. Kouwenhoven, and S. De Franceschi, Science **309**, 272 (2005).
- [11] R. Frielinghaus, I. E. Batov, M. Weides, H. Kohlstedt, R. Calarco, and Th. Schäpers, preprint arXiv:1001.2380v1.
- [12] T. Sand-Jespersen, J. Paaske, B. M. Andersen, K. Grove-Rasmussen, H. I. Jørgensen, M. Aagesen, C. B. Sørensen, P. E. Lindelof, K. Flensberg, and J. Nygård, Phys. Rev. Lett. **99**, 126603 (2007).
- [13] F. K. Wilhelm, G. Schøn, and A. D. Zaikin, Phys. Rev. Lett. **81**, 1682 (1998).
- [14] A. F. Morpurgo, T. M. Klapwijk, and B. H. van Wees, Appl. Phys. Lett. **72**, 966 (1998).
- [15] Th. Schäpers, J. Malindretos, K. Neurohr, S. Lachenmann, A. van der Hart, G. Crecelius, H. Hardtdegen, H. Lüth, and A. A. Golubov, Appl. Phys. Lett. **73**, 2348 (1998).
- [16] J. J. A. Baselmans, A. F. Morpurgo, B. J. van Wees, and T. M. Klapwijk, Nature **397**, 43 (1999).
- [17] A. M. Savin, J. P. Pekola, J. T. Flyktman, A. Anthore, and F. Giazotto, Appl. Phys. Lett. **84**, 4179 (2004).
- [18] F. Giazotto, T. T. Heikkilä, F. Taddei, Rosario Fazio, J. P. Pekola, and F. Beltram, Phys. Rev. Lett. **92** 137001 (2004).
- [19] M. S. Crosser, P. Virtanen, T. T. Heikkilä, and N. O. Birge, Phys. Rev. Lett. **96** 167004 (2006).
- [20] S. Tirelli, A. M. Savin, C. Pascual Garcia, J. P. Pekola, F. Beltram, and F. Giazotto, Phys. Rev. Lett. **101**, 077004 (2008).
- [21] F. Giazotto, T. T. Heikkilä, A. Luukanen, A. M. Savin, J. P. Pekola, Rev. Mod. Phys. **78**, 217 (2006).
- [22] T. T. Heikkilä, J. Särkkä, and F. K. Wilhelm, Phys. Rev. B **66**, 184513 (2002).
- [23] I. O. Kulik and A. N. Omelyan'chuk, Fiz. Nizk. Temp **4**, 296 (1978) [Sov. J. Low Temp. Phys. **4**, 142 (1978)].
- [24] H. Courtois, M. Meschke, J. T. Peltonen, and J. P. Pekola, Phys. Rev. Lett. **101**, 067002 (2008).
- [25] C. Pascual García and F. Giazotto, Appl. Phys. Lett. **94**, 132508 (2009).
- [26] T. D. Clark, R. J. Prance, A. D. C. Grassie, J. Appl. Phys. **51**, 2736 (1980).
- [27] T. Akazaki, H. Takayanagi, J. Nitta, and T. Enoki, Appl. Phys. Lett. **68**, 418 (1996).
- [28] J. J. A. Baselmans, B. J. van Wees, and T. M. Klapwijk, Phys. Rev. B **63**, 094504 (2001).
- [29] M. Meschke, J. T. Peltonen, H. Courtois, and J. P. Pekola, J. Low Temp. Phys. **154**, 190 (2009).
- [30] X. Jiang, Q. Xiong, S. Nam, F. Qian, Y. Li, and C. M. Lieber, Nano Lett. (2007).
- [31] M. Octavio, M. Tinkham, G. E. Blonder, and T. M. Klapwijk, Phys. Rev. B **27**, 6739 (1983).
- [32] M. Tinkham, *Introduction to Superconductivity*, 2nd Edn. (McGraw-Hill, 1996).